Chapter 11
Coupled Biomechanical Modeling of the Face, Jaw, Skull, Tongue, and Hyoid Bone

Ian Stavness, Mohammad Ali Nazari, Cormac Flynn, Pascal Perrier, Yohan Payan, John E. Lloyd and Sidney Fels

11.1 Introduction

Over the past three decades, modeling and simulation of musculoskeletal systems has greatly enhanced our understanding of the biomechanics and neural control of human and animal movement. Musculoskeletal simulations have been used to analyze human posture, gait, reaching, and other motor tasks (for review, see Delp et al. [1]). Musculoskeletal simulations have been reported across multiple spatial scales; however, macro-scale anatomical models have been most prevalent. Such models represent the human body as a series of rigid skeletal components connected by 1D lumped-parameter springs for muscles and tendons. There is increasing interest in modeling human biomechanics at smaller spatial scales and in particular at the tissue-level scale in 3D. These directions are motivated in part by a desire for more

I. Stavness (✉)
Department of Computer Science, University of Saskatchewan,176 Thorvaldson Building, 110 Science Place, Saskatoon, SKS7N 5C9, Canada
e-mail: stavness@gmail.com

M. A. Nazari
Department of Mechanical Engineering, Faculty of Engineering, University of Tehran, Tehran, Iran

C. Flynn
School of Engineering, Science and Primary Industries,Wintec, New Zealand

P. Perrier
Speech & Cognition Department, Gipsa-lab, UMR CNRS 5216, Stendhal University & Grenoble INP, Grenoble, France

Y. Payan
TIMC-IMAG Laboratory, CNRS UMR 5525, University Joseph Fourier, La Tronche, France

J. E. Lloyd · S. Fels
Department of Electrical and Computer Engineering, University of British Columbia,Vancouver, Canada

N. Magnenat-Thalmann et al. (eds.), *3D Multiscale Physiological Human*,
DOI: 10.1007/978-1-4471-6275-9_11,

predictive power in musculoskeletal models, as well as by a desire to simulate more complex anatomical structures.

Tissue-scale muscle models, based on the Finite-Element (FE) method, can capture details regarding internal tissue strain, the wrapping of muscles around bones and other structures, and the transmission of force by muscles with internal connective tissue and broad attachments [2]. The FE modeling paradigm can also be used to represent highly deformable muscular structures such as the face, lips, tongue, and vocal tract, where changes in shape of the structures have functional significance. The face and vocal tract have received less attention by computational biomechanists than the limbs and whole-body. This is likely due to the additional biomechanical complexity of the head and neck anatomy. However, it is this very complexity that makes face and vocal tract systems excellent candidates for simulation in order to elucidate the unique biomechanics of these structures in breathing, feeding, and speaking.

Biomechanical face models have a long history. The earliest physically-based face model was reported by Terzopoulos and Waters [3]. The model was composed of a linear spring-mass mesh and was used to generate compelling animations of facial expression for its time. More recent models have used FE methods to improve the representation of facial tissue and muscle mechanics. Sifakis et al. [4] developed a detailed FE model and simulated speech movements using a kinematically driven jaw. Hung et al. [5] have recently developed a FE face model targeted for visual effects in film. Few previous models have integrated the craniofacial and vocal tract components into a unified simulation. For this reason, much of our modeling efforts have targeted the integration of face and vocal tract anatomy in dynamic simulations [6–11].

Tissue-scale simulations of face and vocal tract biomechanics can be applied in a wide range of domains, including computer animation, medicine, and biology. Much of the previous face modeling work has come out of the computer graphics community in an attempt to create realistic simulations of facial appearance for visual effects in films [3, 4, 12]. Robotic and computer generated faces suffer from the so-called "uncanny valley" phenomenon [13]. This phenomenon, first postulated by Mori in the 70s based on his work building humanlike robots, suggests that as artificial faces become closer to reality they become more eerie and repulsive to a perceiver. Biomechanics-based face simulations have the potential to surpass the uncanny valley, as the facial movements would theoretically mimic the real physical system perfectly. Motion-capture techniques for face animation have improved dramatically for use in computer generated films [14]; however, biomechanics-based face animations have not yet achieved the same level of realism. Synthesizing face animations through simulation without an actor remains an attractive research direction with the potential to reduce the production costs and constraints of motion-capture driven animation.

Biomedical applications of face and vocal tract modeling are also numerous. Dysfunctions in breathing (e.g. obstructive sleep apnea) and feeding (e.g. dysphagia) are thought to involve combined deficits to both the tissue mechanics and neural control of patients. Also, maxillofacial surgeries can benefit from tissue-level craniofacial simulations [15]. For example, simulations can be used to predict the soft-tissue

313863_1_En_11_Chapter ☑ TYPESET ☐ DISK ☐ LE ☑ CP Disp.:12/11/2013 Pages: 22 Layout: T1-Standard

deformations following surgical alteration of the underlying jaw and skull shape [16–18]. Similarly, computer-assisted planning of complex maxillofacial reconstructive surgery has improved outcomes and reduced patient recovery time [19].

Basic questions pertaining to orofacial physiology, such as speech production, can also be investigated with tissue-level simulations. Speech production involves highly coordinated movements of the lips, jaw, and tongue. While speech movements can be analyzed with experimental measurement techniques such as ultrasound, MRI, electromagnetic articulography, electropalatography, and (to a limited extend) electromyography, the principal anatomical structures of the vocal tract are all mechanically coupled. Therefore, in order to understand the neural control of speech articulations, one must account for the role of the intrinsic, coupled mechanics of the articulators.

For simulations to impact the above stated applications, two particular considerations must be addressed. First, many biomedical applications require models that are representative of individual patients. Patient-specific modeling is commonly done to only match the size, shape, and kinematics of a model to a particular patient. For tissue-scale models, the tissue properties should also be matched to the particular patient. Second, face-tissue simulations require integration with the underlying skull and jaw as well as the vocal tract articulators. This is particularly important for modeling speech production because the interactions between the lips and teeth, tongue and teeth, and tongue and jaw position are critical issues. Many applications also require that simulations capture the dynamics of the face and vocal tract structures, because breathing, mastication, swallowing, and speech production are all dynamic acts. The effect of tissue dynamics is more pronounced on fast speed movements, such as speech production, however these effects can also have an impact on slower speed movements.

In order to address these varied modeling requirements and to apply simulations to scientific and clinical questions, we have been developing a set of biomechanical modeling tools as well as a 3D dynamic model of the jaw, skull, tongue, and face. These models were originally developed in the commercial software package ANSYS (www.ansys.com, ANSYS, Inc., Canonsburg, PA) and were more recently re-implemented in the in-house developed software package ArtiSynth (www.artisynth.org, University of British Columbia, Vancouver, Canada). ArtiSynth provides us with flexibility to incorporate state-of-the-art algorithms for very efficient simulations, while ANSYS provides us with a reliable engineering package against which we can corroborate our ArtiSynth simulation results. In this chapter, we provide a description of our tissue-scale modeling approach developed in the ArtiSynth platform. We will focus on aspects of our approach that pertain to the dynamic coupling between the face and vocal tract at the tissue scale. We will also review our results for muscle-driven simulations of speech movements and facial expressions.

11.2 Subject Specific Orofacial Modeling

One of the basic design decisions that we employed in our approach to orofacial modeling was to create a workflow for generating subject-specific face, jaw tongue, skull and hyoid bone models. Subject specificity is important for a number of reasons. Validation of orofacial simulations can be made directly with experimental data from the same subject to which the model is matched. Also, a number of biomedical applications require patient-specific models. Our approach to subject specific modeling involves adapting a set of reference models to a specific subject based on medical imaging data and other clinical measurements. Our subject-specific workflow involves two main components: morphology and material properties.

11.2.1 Subject Specific Morphology

Subject specific morphology involves creating a model with anatomical size and proportions matched to a subject. For whole-body musculoskeletal modeling this typically involves an overall scaling of a generic model to a specific subject [1]. For our purposes with a face and vocal tract model, we require a more detailed type of subject-specific morphology, whereby the shapes of individual bones, muscles, ligaments, and other structures are matched to a subject. This is achieved by adapting the shape of the model's anatomical structures to medical imaging data of a specific subject.

Our workflow for a heterogeneous model, such as the face-jaw-tongue system, involves creating reference models for each model sub-component, adapting the morphology of each sub-component to fit medical imaging data for a single subject and then dynamically attaching the sub-components. In this section, we discuss the reference models for the face, skull, jaw, tongue, and hyoid bone as well as the adaptation process for morphing the reference models into an integrated subject-specific model.

11.2.1.1 Reference Face Model

The reference face model was manually built from a CT dataset of a male subject and has been described in detail elsewhere [20]. This FE model is based on a hexahedral mesh that was carefully constructed to control element quality (such as Jacobian ratio), midsagittal symmetry, and the density of elements such that more elements exist in regions of the face that are known to deform to a greater extent (Fig. 11.1). The mesh includes three layers of elements from superficial to deep. In total, the model includes 6342 hexahedral elements. In this reference model, all layers use an isotropic material, however in the revised model we have implemented an anisotropic passive material in the most superficial layer representing the epidermis and dermis (as described below in the *Anisotropic in-vivo measurements* section).

313863_1_En_11_Chapter ☑ TYPESET ☐ DISK ☐ LE ☑ CP Disp.:12/11/2013 Pages: 22 Layout: T1-Standard

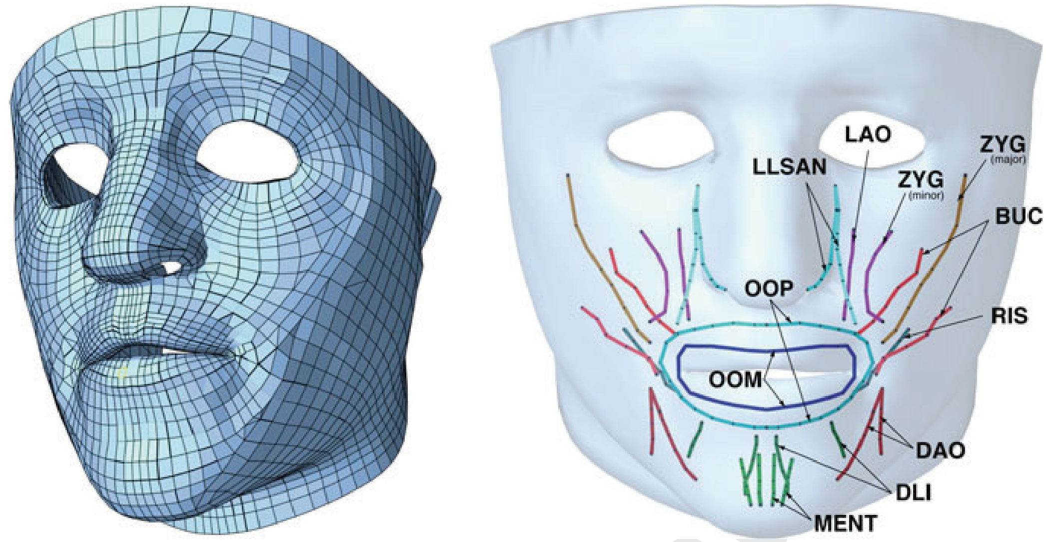

Fig. 11.1 The reference finite-element face model. Muscles include the levator labii superioris alaeque nasi (LLSAN), levator anguli oris (LAO), zygomaticus (ZYG), buccinator (BUC), risorius (RIS), depressor anguli oris (DAO), depressor labii inferioris (DLI), mentalis (MENT), orbicularis oris peripheralis/marginalis (OOP/M)

The muscles of the face are represented in the reference model with line-based muscles called "cable-elements" embedded within the model that apply muscle forces onto the FE mesh. Importantly, these cable elements include stress-stiffening effects of muscle contraction [9, 20]. Our revised face model uses transversely-isotropic muscle materials with muscle elements chosen within a volume surrounding the original cable elements and fiber directions consistent with the cable directions.

11.2.1.2 Reference Jaw-Skull-Hyoid Model

The reference jaw-skull-hyoid model was developed to simulate muscle-driven masticatory movements in ArtiSynth. The model is pictured in Fig. 11.2 and has been described in detail elsewhere [21]. It includes rigid-bodies for the skull, jaw, and hyoid bone derived from cone-beam CT data. The inertia of the jaw and hyoid were computed from the bone shapes, assuming uniform density of 3600 and $2000\,\mathrm{kg/m^3}$ for the jaw and hyoid respectively. Curvilinear constraint surfaces are included to represent the articular surfaces of the temporomandibular joints. Planar contact surfaces are used to represent teeth contact.

The model includes 30 Hill-type line muscles to represent the main compartments of the mandibular muscles. Muscle properties, including maximum cross-sectional area and fiber lengths, are based on previous anatomical and modeling studies [22]. The origin and insertion points for each muscle are specified according to anatomical landmarks. The hyoid bone is attached to a fixed larynx with a linear translational/rotational spring representing the hyothyroid membrane and ligament.

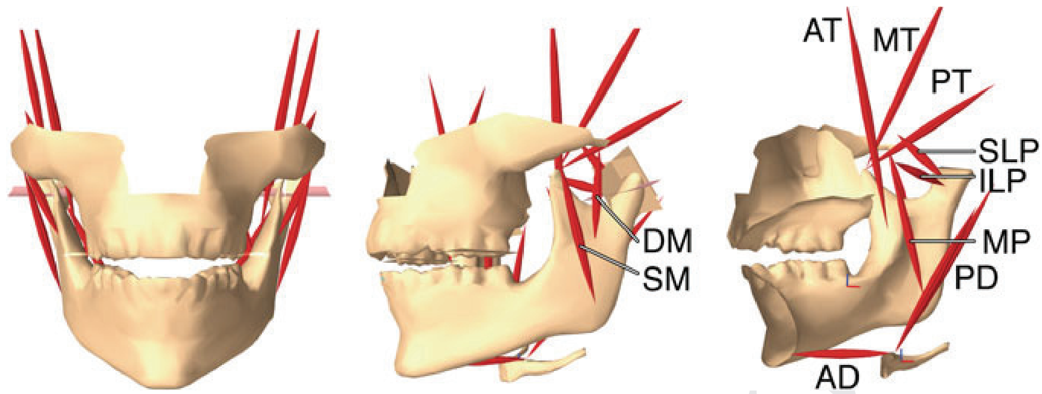

Fig. 11.2 The subject-specific rigid-body jaw-maxilla-hyoid model. Muscles include the deep/superficial masseter (D/SM), anterior/middle/posterior temporalis (A/M/PT), superior/inferior lateral pterygoid (S/ILP), medial pterygoid (MP) and posterior/anterior belly of the digastric (P/AD). From Ref. [8]. Copyright 2011 by John Wiley & Sons, Ltd. Reproduced with permission

11.2.1.3 Reference Tongue Model

The reference FE tongue model was originally developed by Gerard et al. [6] and Buchaillard et al. [7] in ANSYS and subsequently re-implemented by Stavness et al. [8] in ArtiSynth. It is pictured in Fig. 11.3. The shape of the reference tongue model is based on CT and MRI data for a single male subject. The model's FE mesh includes 740 hexahedral elements with a density of 1040 $\mathrm{kg/m^3}$ for a total tongue mass of 106 g.

The FE mesh was constructed to approximate the shape of the lingual muscles. Therefore, in the reference model, muscle fiber directions are specified along the edges of the FE mesh. Our revised model uses transversely-isotropic muscle materials with fiber directions consistent with the original reference model.

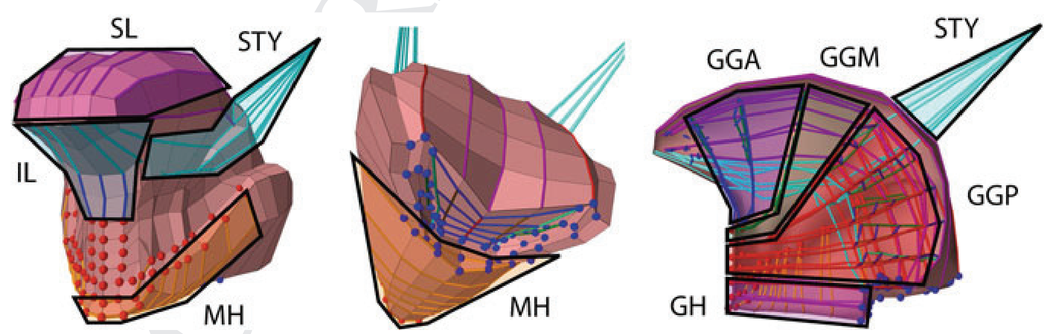

Fig. 11.3 The subject-specific finite-element tongue model. Muscles include the superior/inferior longitudinal (S/IL), mylohyoid (MH), styloglossus (STY), geniohyoid (GH), anterior/middle/posterior genioglossus (GGA/M/P), as well as the transverse, vertical, and hyoglossus muscles (not shown). From Ref. [8]. Copyright 2011 by John Wiley & Sons, Ltd. Reproduced with permission

11.2.1.4 Adaptation to Subject Morphology

In order to create a unified model of the face, skull, jaw, tongue, and hyoid bone with the morphology of a single subject, we used an adaptation procedure to morph the skeletal and muscle geometries of reference models to fit a CT dataset. The 3D jaw, skull, and hyoid surface meshes were adapted to a 3D skull surface segmented from CT data. Symmetry was attained by mirroring the left-side of the registered meshes. The reference face model was adapted based on the boundary conditions of the skull surface and the outer air-skin surface segmented from the CT data. The reference tongue model was originally constructed based on the CT data and therefore adaptation was not required.

The adaptation process used a non-elastic mesh-based registration algorithm called MMRep [23, 24], which is automatically driven in order to conform the surface meshes of two models. Additional control points were used to enforce particular correspondences between the models. Importantly, for FE models, the MMRep algorithm attempts to maintain element regularity during the adaptation process, and thus the adapted FE face mesh maintained sufficient element quality for use in FE analysis.

The automatic adaptation to CT data achieved satisfactory results for the main features of the model (Fig. 11.4). However, the lip region of the model was found not to conform well. Discretization artifacts of the CT voxel data caused the lip region to become unrealistically flat. Manual node-by-node registration was performed in the region of the lip with guidance from the original CT dataset [10]. This fine-tuning was important only for detailed simulations of lip protrusion.

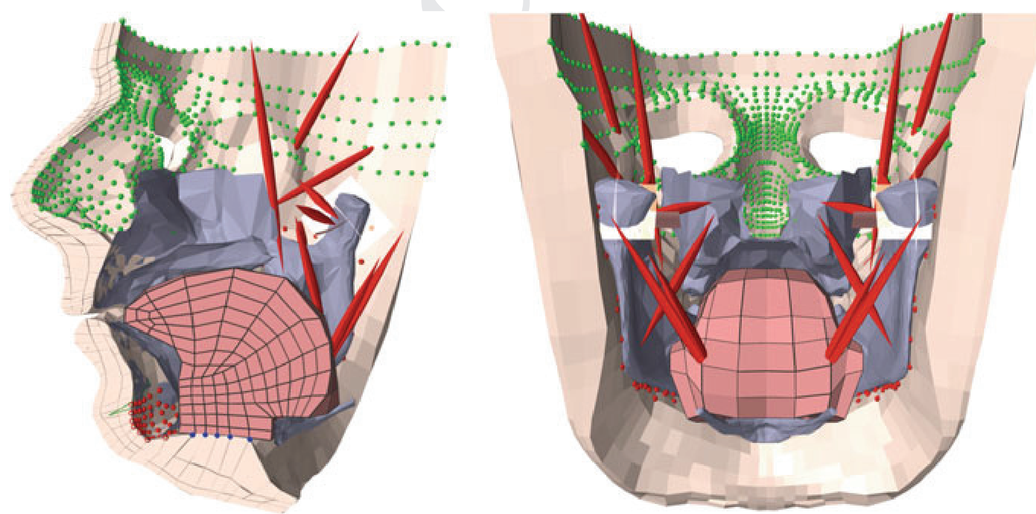

Fig. 11.4 The registered and coupled face-jaw-tongue-hyoid model. From Ref. [10]. Copyright 2013 by American Speech-Language-Hearing Association. Adapted with permission

313863_1_En_11_Chapter ☑ TYPESET ☐ DISK ☐ LE ☑ CP Disp.:12/11/2013 Pages: 22 Layout: T1-Standard

11.2.1.5 Face-Jaw-Tongue Attachments

The insertion sites of the facial and lingual muscles define the primary attachments between the face, jaw, and tongue models. Line-based mandibular muscles couple the hyoid bone to the jaw and skull. These include the digastrics, stylohyoid, and geniohyoid muscles. The tongue is coupled to the jaw and hyoid bone by node attachments and by the end-points of the genioglossus and mylohyoid muscles. These attachments are implemented with the nodes of the muscle elements in the FE model.

The face muscles are attached to the underlying jaw and skull with node attachments. In addition, a number of inner-surface nodes of the face are attached to the jaw and maxilla to represent the zygomatic and mandibular ligaments. The nodes in the region of the lips and cheeks are unattached. Adjacent surfaces of the tongue and face models are attached near the region of the floor of the mouth. The attachment points are illustrated in Fig. 11.5.

Contact between the upper and lower lip, the lips and the teeth, the tongue and jaw, and the tongue and hard-palate are also implemented in the model. Unlike attachment constraints, which are always coupling the tissues together, contact constraints are only active when the meshes of the structures are in contact. Contact handling is described below.

11.2.2 Subject Specific Material Properties

In addition to subject specific morphology, material properties are also required for a biomechanical model. Subject specific material properties are much more challenging to acquire than morphology because experimental techniques for measur-

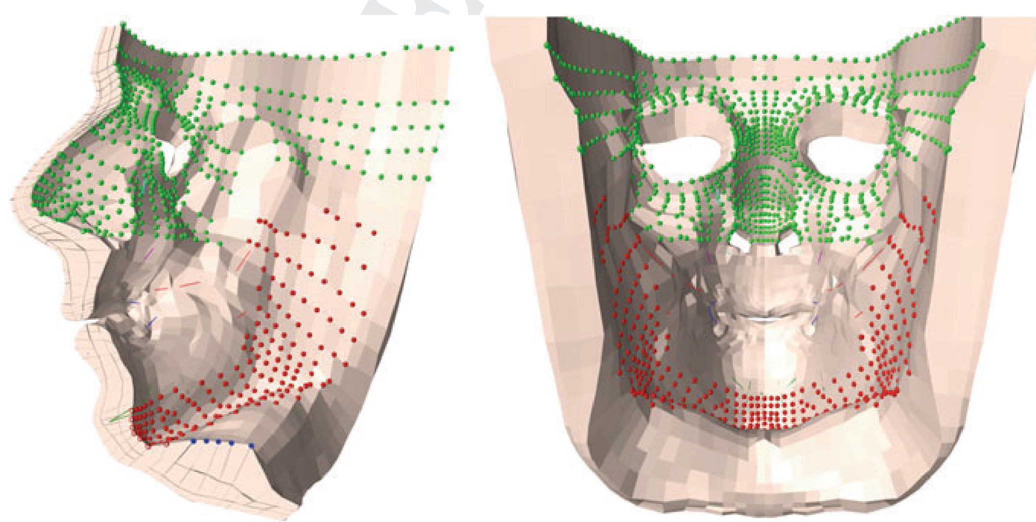

Fig. 11.5 Attachment points between the face and underlying bony structures. From Ref. [10]. Copyright 2013 by American Speech-Language-Hearing Association. Adapted with permission

ing tissue mechanics are much less routine than medical imaging for morphology. Our reference models incorporate average material properties from cadaver studies and previously published literature. Recently, we have worked with collaborators to develop new experimental protocols to measure subject-specific material properties in vivo [25, 26]. Our general approach for representing soft-tissue mechanics is to combine a passive matrix for tissue elasticity together with along-fiber muscle mechanics using an uncoupled strain energy formulation [27, 28].

11.2.2.1 Isotropic Indentation Measurements

The initial material properties for our FE models were taken from literature data in combination with mechanical testing with fresh cadaveric cheek and tongue tissues [29]. The mechanical testing involved uniaxial indentation tests using an EnduraTEC indentation device (Bose Corporation, Framingham, MA). The experimental setup is pictured in Fig. 11.6. Indentation measurements characterized the relationship between the local force applied to the external surface of the tissue and the resulting displacement. These measurements were used to fit parameters in a isotropic, non-linear, hyperelastic material—a fifth-order Mooney-Rivlin material [30, 31],

$$W = C_{10}\,(I_1 - 3) + C_{20}\,(I_1 - 3)^2 + \frac{\kappa}{2}\,(\ln J)^2\,,$$

where the $\kappa/2\,(\ln J)^2$ term enforces tissue incompressibility. Other terms in the Mooney-Rivlin material were omitted, i.e. $c_{01} = c_{11} = c_{02} = 0$. For the face tissue, material coefficients were found of $c_{10} = 2500\,\text{Pa}$, $c_{20} = 1175\,\text{Pa}$ [20]. For the tongue tissue, material coefficients were found of $c_{10} = 1037\,\text{Pa}$, $c_{20} = 486$ Pa

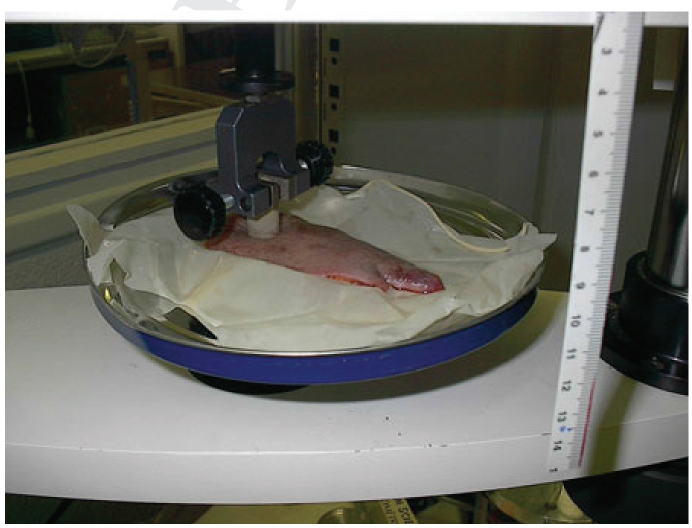

Fig. 11.6 Experimental setup for indentation-based mechanical testing of cheek and tongue tissue

[7]. Both models had a density of $1040\,\mathrm{kg/m^3}$ and used Rayleigh damping, which is a viscous damping proportional to both tissue stiffness (β coefficient) and tissue mass (α coefficient). Rayleigh damping coefficients were set to achieve critically damped response for each model ($\beta = 0.055\,\mathrm{s}$ and $\alpha = 19\,\mathrm{s}^{-1}$ for the face model, and $\beta = 0.03\,\mathrm{s}$ and $\alpha = 40\,\mathrm{s}^{-1}$ for the tongue model).

11.2.2.2 Anisotropic In-vivo Measurements

Recently, we have characterized the mechanical behavior of in vivo facial skin using a combined experimental and numerical approach [25]. The facial skin of the central cheek area of five subjects was characterized. Five additional locations on the face were also characterized for one of the subjects. To the best of our knowledge, these are the first reported values of in vivo facial pre-stresses in the literature.

For the experiment, a region of interest on the subject's face was isolated with a boundary ring with inside diameter of 37.5 mm. A micro-robot applied a rich set of deformation cycles at 0.1 Hz to the skin surface via a 4 mm cylindrical probe (Fig. 11.7). The probe was attached using liquid cyanoacrylate adhesive to the surface of the skin. A series of in-plane deformations was applied followed by a series of out-of-plane deformations. The probe position and reaction force were measured and recorded along with a time-stamp for each data point.

For the numerical simulation, an FE simulation of the experiment was used in an optimization framework to find material parameters and pre-stresses that best-fit the model data to the experimental data from each subject and each facial region. The FE model was developed in ANSYS using an Ogden strain energy function to represent the skin and a quasi-linear viscoelastic law [32] to model the dissipative characteristics of skin. During the first load-step of the analysis an orthogonal pre-

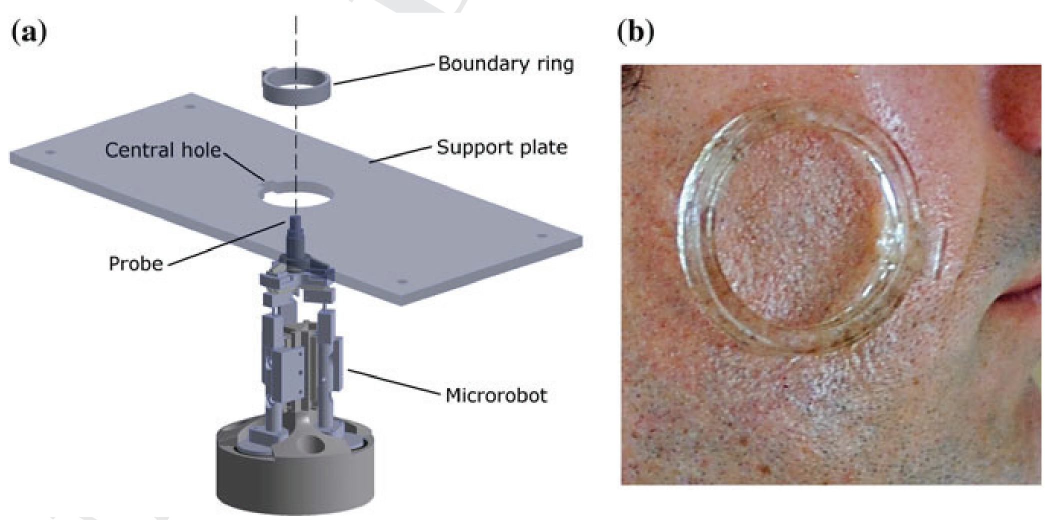

Fig. 11.7 **a** Robotic probe for in vivo mechanical testing, **b** boundary ring attached to volunteer's central cheek area. From Ref. [25]. Copyright 2013 by Elsevier. Adapted with permission

stress was applied representing the in vivo tension inherent in human skin. After the pre-stress was applied the domain was remeshed such that the diameters of the large and small partitions were 37.5 and 4 mm, respectively. For the second step of the analysis, all nodes outside the 37.5 mm diameter partition were fixed. The nodes inside the probe area were moved according to the protocol in the experiment. The total sum of the nodal reaction forces in the probe region was calculated.

The measured force-displacement response for all tests was non-linear, anisotropic, and viscoelastic (Fig. 11.8). There was a large inter-subject variation in the skin stiffness of the central cheek area and also a large intra-subject variation in the skin stiffness at different facial locations. The direction in which the force-displacement response was stiffest at each location corresponded to the reported direction of Relaxed Skin Tension Lines (RSTL) [33] at that location. The one exception to this was the forehead region, where the direction of stiffest response was orthogonal to the RSTL direction.

The finite element model simulated the non-linear, anisotropic, and viscoelastic behaviour of the skin observed in the experiments (Fig. 11.8). The error-of-fit between the model and experiments ranged from 12 to 23 %. The in vivo stresses ranged from 15.9 to 89.4 kPa.

11.2.2.3 Muscle Materials

To represent muscle mechanics in the FE face and tongue models we used a transverse-isotropic muscle material based on the constitutive equation proposed by Blemker et al. [27]. This type of material has stiffness properties in the direction along the muscle fiber that differ from properties in the directions orthogonal to

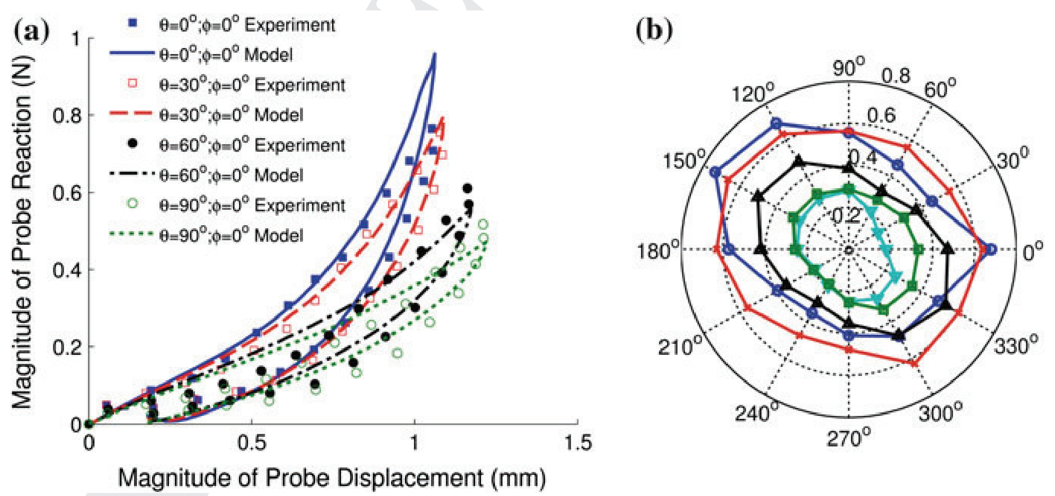

Fig. 11.8 **a** Comparison of experimental and model force-displacement response of forehead region of one volunteer, **b** force at 1.1 mm displacement in different in-plane directions for all central cheek area of all volunteers. From Ref. [25]. Copyright 2013 by Elsevier. Adapted with permission

it. Passive stress along the fiber direction was made to increase exponentially with increasing fiber stretch (see Weiss et al. [28], Eq. 7.2, p. 123). Parameters for the constitutive model were taken to be consistent with Blemker et al. [27]: $\lambda^* = 1.4$ (the along fiber stretch at which collagen fibers are straightened), $C_3 = 0.05$ (scales the exponential stresses) and $C_4 = 6.6$ (rate of uncrimping of the collagen fibers). The maximum active fiber stress was 100 kPa.

11.3 Coupled Rigid-Body/FE Modeling

Simulating orofacial biomechanics is particularly challenging because of the mechanical coupling between relatively hard structures (such as the jaw, skull, and teeth) and relatively soft structures (the face, tongue, soft-palate, and vocal tract). Previous models of the face, jaw, and tongue have largely neglected these coupling effects, but we have shown these effects to be significant [8]. In this section, we discuss the simulation methods that we have developed in ArtiSynth for coupled simulation of our face-jaw-tongue model. The main components of the simulator necessary for face and vocal tract simulations are: (1) FE simulation, (2) coupling and (3) contact handling.

11.3.1 Finite-Element Simulation

ArtiSynth is an interactive simulation platform that combines multibody models, composed of rigid bodies connected by joints, with FE models composed of nodes and elements. The physics solver is described in detail in Sect. 11.4 of Lloyd et al. [34].

The positions, velocities, and forces for all rigid bodies (6 DOF) and FE nodes (3 DOF) are described respectively by the composite vectors **q, u**, and **f**. Likewise, we have a composite mass matrix **M**. The forces **f** are the sum of external forces and internal forces due to damping and elastic deformation. Simulation consists of advancing **q** and **u** through a sequence of time steps k with step size h. The velocity update is determined from Newton's Law, which leads to update rules such as the first order Euler step $\mathbf{M}\mathbf{u}^{k+1} = \mathbf{M}\mathbf{u}^k + h\mathbf{f}^k$. In addition, we enforce both bilateral constraints (such as joints or incompressibility) and unilateral constraints (such as contact and joint limits), which respectively lead to constraints on the velocities given by $\mathbf{G}\mathbf{u}^{k+1} = 0$ and $\mathbf{N}\mathbf{u}^{k+1} \geq 0$, where **G** and **N** are the (sparse) bilateral and unilateral constraint matrices. These constraints are enforced over each time step by impulses $\boldsymbol{\lambda}$ and **z** acting on $\mathbf{G}^T$ and $\mathbf{N}^T$, so that the velocity update becomes

$$\mathbf{M}\mathbf{u}^{k+1} = \mathbf{M}\mathbf{u}^k + h\mathbf{f}^k + \mathbf{G}^T\boldsymbol{\lambda} + \mathbf{N}^T\mathbf{z}. \tag{11.1}$$

313863_1_En_11_Chapter ☑ TYPESET ☐ DISK ☐ LE ☑ CP Disp.:12/11/2013 Pages: 22 Layout: T1-Standard

The presence of FE models means that the system is often stiff, requiring the use of an implicit integration step where an approximation of $\mathbf{f}^{k+1}$ is used in place of $\mathbf{f}^{k}$. This can be achieved by replacing $\mathbf{M}$ and $\mathbf{f}^{k}$ in (11.1) with $\hat{\mathbf{M}}$ and $\hat{\mathbf{f}}^{k}$, which contain additional terms derived from the force Jacobians $\partial\mathbf{f}/\partial\mathbf{q}$ and $\partial\mathbf{f}/\partial\mathbf{u}$ [34]. Combining all this into a matrix form with the constraint conditions leads to a mixed linear complementarity problem (MLCP), which we solve at each time step:

$$\begin{pmatrix} \hat{\mathbf{M}} & -\mathbf{G}^{\mathbf{T}} & -\mathbf{N}^{T} \\ \mathbf{G} & 0 & 0 \\ \mathbf{N} & 0 & 0 \end{pmatrix} = \begin{pmatrix} \mathbf{u}^{k+1} \\ \boldsymbol{\lambda} \\ \mathbf{z} \end{pmatrix} + \begin{pmatrix} \mathbf{M}\mathbf{u}^{k} + h\hat{\mathbf{f}} \\ \mathbf{g} \\ \mathbf{n} \end{pmatrix} = \begin{pmatrix} 0 \\ 0 \\ \mathbf{w} \end{pmatrix}$$

$$0 \leq \mathbf{z} \perp \mathbf{w} \geq 0. \tag{11.2}$$

Here $\mathbf{g}$ and $\mathbf{n}$ arise from the time derivatives of $\mathbf{G}$ and $\mathbf{N}$, $\mathbf{w} \equiv \mathbf{N}\mathbf{u}^{k+1}$, and the complementarity condition $0 \leq \mathbf{z}\perp\mathbf{w} \geq 0$ arises from the fact that for unilateral constraints, $\mathbf{z} > 0$ and $\mathbf{N}\mathbf{u}^{k+1} > 0$ must be mutually exclusive. The system (11.2) is also applicable to higher order integrators such as the trapezoidal rule [34], and is also used to compute position corrections $\delta\,\mathbf{q}$ that remove errors due to constraint drift and contact interpenetration.

11.3.2 Coupling FE Models and Rigid Bodies

In models such as our orofacial model, it is necessary to connect FE models to other FE models and rigid bodies. In ArtiSynth, connecting FE and rigid-body is done using point-based attachments, whereby an FE node is attached either to another FE node, an FE element, or a rigid body. In all cases, this results in the state (position and velocity) of the attached node becoming an explicit function of the states of several other nodes or bodies. If we let β denote the set of all attached nodes, and α denote all unattached (or *master*) nodes and bodies, and denote these sets' respective velocities by $\mathbf{u}_\beta$ and $\mathbf{u}_\alpha$, then at any time $\mathbf{u}_\beta$ can be determined by the velocity constraint

$$\mathbf{u}_\beta + \mathbf{G}_{\beta\,\alpha}\mathbf{u}_\alpha = \mathbf{0}$$

where $\mathbf{G}_{\beta\,\alpha}$ is time varying and sparse. In other words, attachments can be implemented as a special kind of bilateral constraint. If we partition system (11.2) into the sets β and α, let $\mathbf{b} \equiv \mathbf{M}\mathbf{u}^{k} + h\hat{\mathbf{f}}$, and ignore unilateral constraints for simplicity, we obtain

$$\begin{pmatrix} \hat{\mathbf{M}}_{\alpha\,\alpha} & \hat{\mathbf{M}}_{\alpha\,\beta} & -\mathbf{G}^{T}_{\alpha\,\alpha} & -\mathbf{G}^{T}_{\beta\,\alpha} \\ \hat{\mathbf{M}}_{\beta\,\alpha} & \hat{\mathbf{M}}_{\beta\,\beta} & -\mathbf{G}^{\mathbf{T}}_{\alpha\,\beta} & -\mathbf{I} \\ \mathbf{G}_{\alpha\,\alpha} & \mathbf{G}_{\alpha\,\beta} & 0 & 0 \\ \mathbf{G}_{\beta\,\alpha} & \mathbf{I} & 0 & 0 \end{pmatrix} \begin{pmatrix} \mathbf{u}^{k+1}_{\alpha} \\ \mathbf{u}^{k+1}_{\beta} \\ \boldsymbol{\lambda}_\alpha \\ \boldsymbol{\lambda}_\beta \end{pmatrix} = \begin{pmatrix} \mathbf{b}_\alpha \\ \mathbf{b}_\beta \\ \mathbf{g}_\alpha \\ \mathbf{g}_\beta \end{pmatrix}. \tag{11.3}$$

The presence of the identity matrices in this system makes it easy to solve for $\mathbf{u}_\beta^{k+1}$ and $\boldsymbol{\lambda}_\beta$ as

$$\mathbf{u}_\beta^{k+1} = \mathbf{g}_\beta - \mathbf{G}_{\beta\alpha}\mathbf{u}_\alpha^{k+1},$$

$$\boldsymbol{\lambda}_\beta = -\mathbf{b}_\beta + (\hat{\mathbf{M}}_{\beta\alpha} - \hat{\mathbf{M}}_{\beta\beta}\mathbf{G}_{\beta\alpha})\mathbf{u}_\alpha^{k+1} + \hat{\mathbf{M}}_{\beta\beta}\mathbf{g}_\beta - \mathbf{G}_{\alpha\beta}^T\boldsymbol{\lambda}_\alpha$$

and therefore condense (11.3) into a reduced system

$$\begin{pmatrix} \hat{\mathbf{M}}' & -\mathbf{G}'^T \\ \mathbf{G}' & 0 \end{pmatrix} \begin{pmatrix} \mathbf{u}_\alpha^{k+1} \\ \boldsymbol{\lambda}_\alpha \end{pmatrix} = \begin{pmatrix} \mathbf{b}' \\ \mathbf{g}'_\alpha \end{pmatrix}.$$

11.3.3 Contact Handling

Contact handling is another important feature of our face model, in particular the ability to handle contact between FE models (e.g. tongue/lips contacts) and other FE models or rigid bodies (e.g. tongue/teeth contacts). In ArtiSynth, contact involving FE models is based on interpenetration of the surface nodes. First, the surface meshes of the respective bodies are intersected to determine which FE surface nodes are interpenetrating. A constraining direction is then determined for each interpenetrating node, based on the normal of the opposing face closest to that node (see Fig. 11.9). These directions are then used to form velocity constraints between the interpenetrating nodes and the opposing faces. These constraints are then added to system (11.2) for the subsequent time step to prevent the resulting velocity from increasing the interpenetration, and they are also used to solve for the nodal displacements required to correct the initial interpenetration.

In principle, these nodal constraints should be unilateral constraints. However, because they are relatively decoupled, it is usually possible to implement them as temporary bilateral constraints for the duration of the next time step, with the constraints being removed after the time step if the computed impulse indicates that the contact is trying to separate. This significantly improves computation time, since bilateral constraints in (11.2) are much faster to solve than unilateral constraints.

11.4 Applications of Biomechanical Face Modeling

Biomechanical face modeling permits a wide range of applications, as discussed in the introduction to this chapter. Thus far, we have focused our simulation studies on coupled face-jaw actions. In particular, we have used simulations to analyze the biomechanics of lip rounding and protrusion, lip closure, and facial expressions.

313863_1_En_11_Chapter ☑ TYPESET ☐ DISK ☐ LE ☑ CP Disp.:12/11/2013 Pages: 22 Layout: T1-Standard

11.4.1 Lip Stiffness Enables Protrusion and Rounding

One motivation for our face modeling efforts was to better understand the biomechanics underlying speech articulations with the lips. The production of rounded vowels in speech, such as /u/, /o/, or /y/ in French, requires a small area of opening between the upper and lower lip. Although a small lip opening could be generated in a number of different ways, many speakers achieve it by protruding the lips. The regularity of this speech articulation across speakers suggests that protrusion is an efficient way to achieve small lip opening areas. We were interested in using biomechanics simulation to analyze how the intrinsic properties of lip muscles could enable small lip aperture through lip protrusion during rounded vowel production [9].

Stiffness is an intrinsic property of muscle tissue. It increases with muscle activation, which is known as the "stress-stiffening" effect. In order to assess the role of intrinsic muscle stiffness, we simulated lip-rounding movements with and without stress-stiffening effects. Simulations were performed by activating the orbicularis oris (OO) muscle in the model and results are shown in Fig. 11.10. Simulations showed that a proper protrusion and rounding lip gesture was achieved by including stress-stiffening in the OO muscle. A saturation effect was also observed such that for a sufficient level of stiffness, lip protrusion and rounding was maintained as the OO activation level increased. Likewise, with a sufficient amount of OO activation, the lip gesture was maintained as the magnitude of stiffness increased. The differences in resulting lip shapes for simulations with and without stiffening were sufficient to affect the spectral characteristics of the speech signal obtained for the French vowel /u/. This result suggests that a simple strategy to generate protruded and rounded lips could be to activate the OO muscle while stiffening the tissues [9].

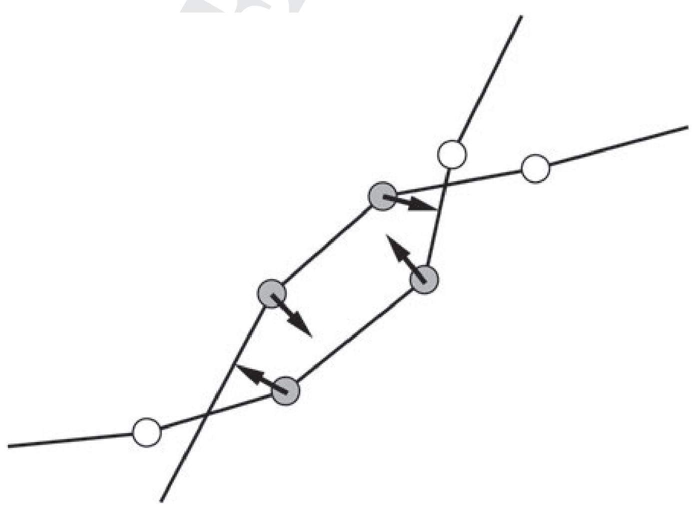

Fig. 11.9 Contact handling between two deformable models, shown schematically in 2D, with inter-penetrating nodes shown in *grey* and the associated constraint directions shown using *arrows*

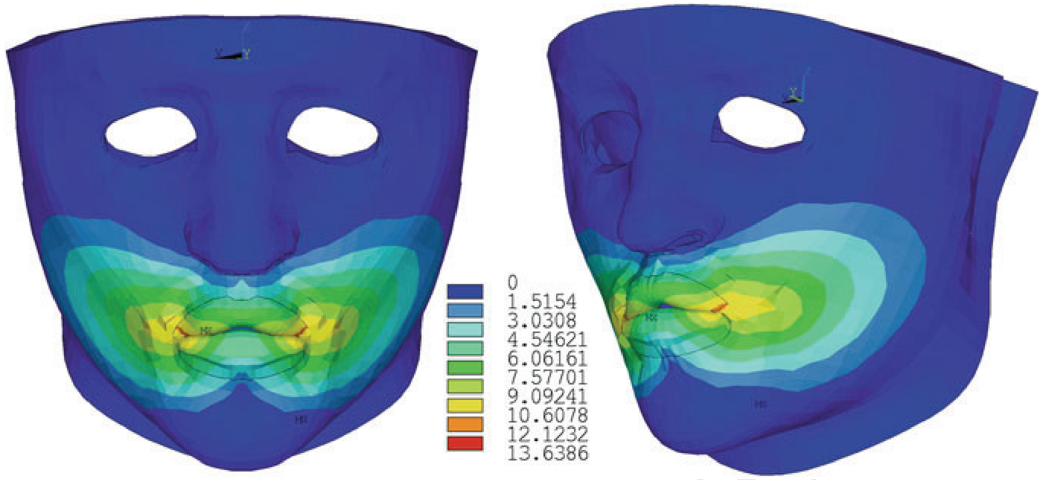

Fig. 11.10 Stress stiffening of the orbicular oris muscles enables a protrusive rounding gesture of the lips. *Color plot* shows tissue displacement from rest (mm)

11.4.2 Lip Morphology Affects Protrusion and Rounding

Having shown that the stiffness of the OO muscle is an important factor in lip rounding and protrusion, we also expected that the morphology of the muscle would be an important factor. Face morphology, including face muscle size and structure, is known to vary between individuals and across different populations. These differences could potentially account for variations in face shapes and speech sounds that are found in different languages across the world. We evaluated our hypothesis by simulating lip protrusion and rounding with various configurations of the OO muscle [10].

The OO muscle was modeled as a continuous loop of muscle elements around the lips. We varied the deepness and peripheralness of this ring of muscles, simulated lip rounding and protrusion, and observed differences in resulting lip shapes. In general, we found that activating the more peripheral region of the OO muscle resulted in greater lip protrusion.

Simulation results of lip protrusion for different configurations of OO muscle geometry are shown in Fig. 11.11 for the same level of activation of the muscle elements. General trends in the simulation results showed that more peripheral OO implementations were associated with larger protrusion, independent of deepness. The degree of deepness seemed to influence the covariation of protrusion and lip area. For a deep OO implementation, peripheralness and protrusion were systematically associated with larger lip width and lip height, and therefore with larger lip area. For a superficial implementation, peripheralness was also associated with larger lip area, mainly due to an increase in lip width. Also, a superficial implementation seemed to be inappropriate for generating protrusion and rounding and instead facilitated lip-closing gestures.

313863_1_En_11_Chapter ☑ TYPESET ☐ DISK ☐ LE ☑ CP Disp.:12/11/2013 Pages: 22 Layout: T1-Standard

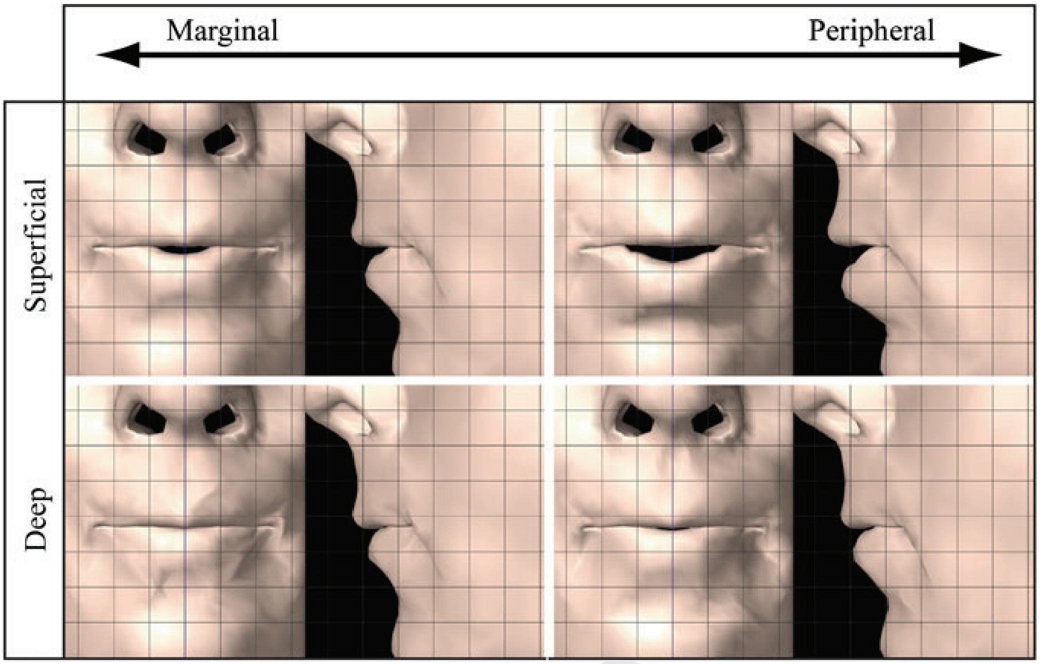

Fig. 11.11 Regional activation of the orbicularis oris muscle (deep vs. superficial and marginal vs. peripheral) changes the shape of the lips, the degree of opening, and the magnitude of protrusion for the same level of muscle activation. From Ref. [10]. Copyright 2013 by American Speech-Language-Hearing Association. Adapted with permission

11.4.3 Teeth Support Lip Protrusion

In addition to intrinsic properties and morphology of the lip muscles, we also expected that mechanical coupling with the underlying rigid structures of the jaw, maxilla and teeth are needed to provide the mechanical support necessary for lip protrusion. We tested this hypothesis by simulating two conditions: lip protrusion with and without teeth support. Such conditions are straight-forward to simulate because contact constraints in the model can be turned off, in which case there is no resistance to the lips from interpenetrating the teeth and vice versa.

Simulations are shown in Fig. 11.12 and were found to support our hypothesis of the importance of skeletal support. The lack of skeletal and teeth support resulted in reduced protrusion of the lips and was generally disruptive of the rounding gesture.

11.4.4 Jaw Opening and Lip Closure

We believe that coupling of the jaw and face is a functionally important aspect of speech movements. We expected that jaw opening would affect the lips, e.g. by reducing the capacity to produce lip closure due to this coupling. Lip closure is known to be possible even at low jaw positions during speech movements such as bilabial consonants /b/ or /p/ [35]. Through simulation, we wanted to assess which

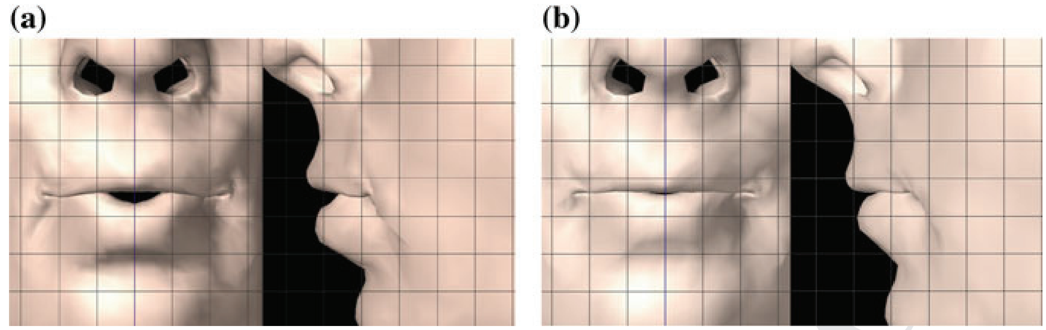

Fig. 11.12 **a** Lip protrusion is achieved with skeletal support, **b** lip protrusion is reduced without mechanical support of the underlying bone structures of the jaw, maxilla, and teeth

parts of the OO muscle would be activated to best achieve a closure for low jaw postures [10].

Our simulations showed that activating the superficial layer of the OO muscle was best suited for achieving lip closure for a low jaw posture. The results are plotted in Fig. 11.13. The additional recruitment of middle, marginal portion achieved a lip closure with a very low jaw posture. The peripheral OO activation provided the required closure of the lips by downward movement of the upper lip and upward movement of the lower lip. Notably, we also observed coupling effects between the face and jaw: activation of OO to achieve lip closure induced a slight jaw closure. These simulations demonstrated that lip closure is compatible with variable jaw heights [10].

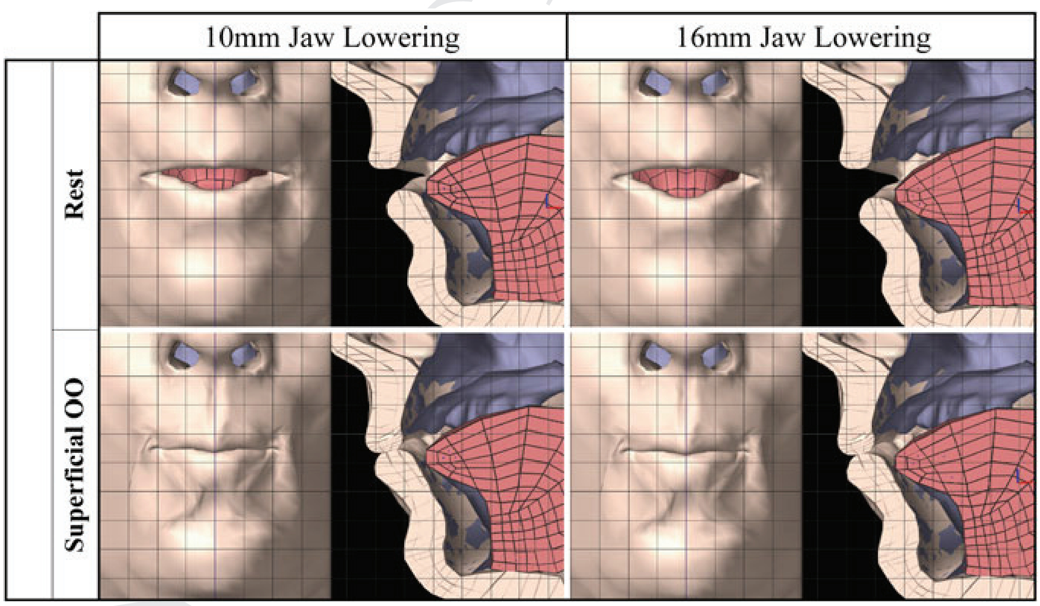

Fig. 11.13 Lip closure is achieved for an open jaw posture with activation of the superficial region of the orbicularis oris muscle. From Ref. [10]. Copyright 2013 by American Speech-Language-Hearing Association. Adapted with permission

11.4.5 Facial Expression Simulations

We also used our face-jaw-tongue-hyoid model to simulate a series of facial expressions and compared the displacement of landmarks with experimental measurements in the literature [11]. For these simulations, the hypodermis, represented by the inner and middle layer of elements in the face model, was simulated using a Mooney-Rivlin material. The outer layer of elements representing the epidermis and dermis was modeled using an anisotropic material with parameters based on in vivo tests as described above.

For these simulations, a novel aspect of the face model was the imposition of a pre-stress corresponding to the tension inherent in living skin. The inner nodes of the facial elements were scaled prior to the finite element analysis. During the first step of the analysis, they were displaced back to their reference positions. This resulted in a tension field similar to the RSTLs observed by Borges [33].

The simulated facial expressions included a closed-mouth smile, an open-mouth smile, pursing of the lips, and lips turned downwards (Fig. 11.14). These were achieved by activating appropriate sets of orofacial muscles. For all facial expressions, the mouth corner experienced the largest displacement, which was in agreement with experimental observations. The simulated landmark displacements were within a standard deviation of the measured displacements (Fig. 11.15). For open and closed-mouth smiles, increasing the stiffness of the skin layer resulted in smaller landmark displacements (Fig. 11.15). Increasing the in vivo skin tension had a variable effect on landmark displacements.

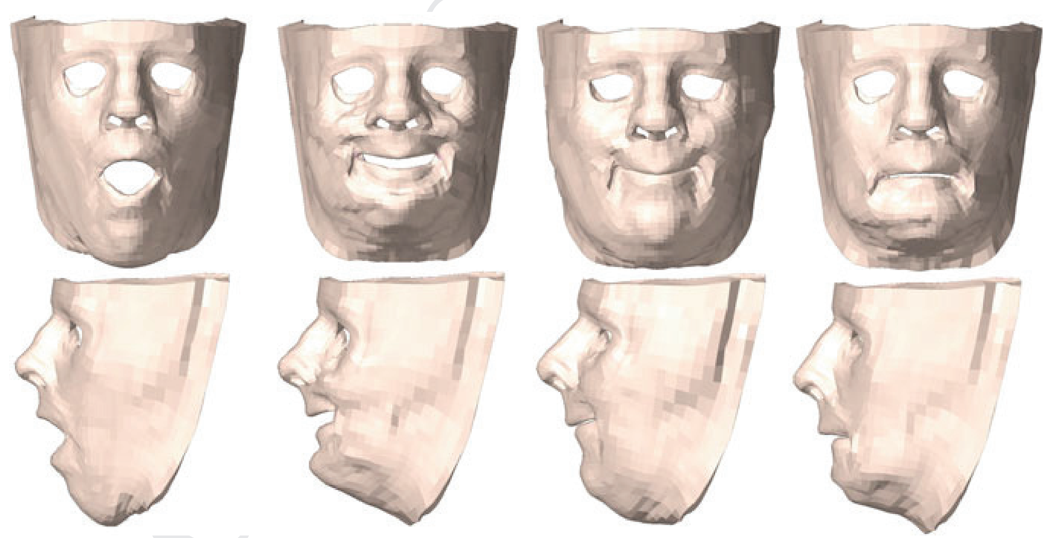

Fig. 11.14 Muscle-driven simulations of different facial expressions. From Ref. [11]. Copyright 2013 by Taylor & Francis. Adapted with permission

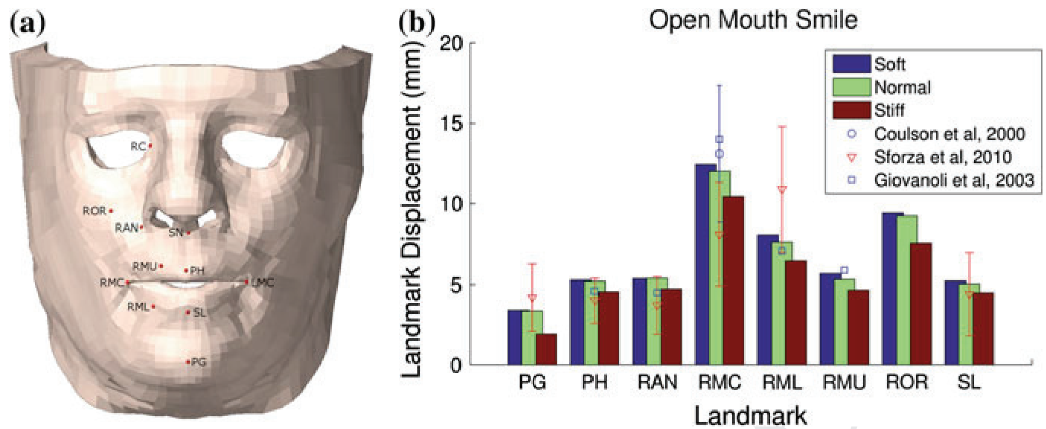

Fig. 11.15 **a** Facial landmarks, **b** landmark displacements for an open-mouth smile with different skin-types. From Ref. [11]. Copyright 2013 by Taylor & Francis. Adapted with permission

11.5 Summary

In summary, tissue-scale modeling of musculoskeletal systems involves a number of engineering challenges and presents a number of high impact applications in biomechanics and computer animation. In this chapter we have presented an approach to simulating coupled hard and soft tissue biomechanical systems at the tissue scale through combined finite-element analysis with multi-body dynamics. We have demonstrated our approach for simulating face-jaw-tongue movements. Our approach is generally applicable to modeling musculoskeletal systems other than the head and neck, and we are currently pursuing simulations studies with tissue-scale models of the upper extremity [36].

Future directions for this work include new computational techniques to improve simulation speed as well as additional experimental work to refine the model and validate simulations. Measuring muscle activations for facial expressions and lip articulations would provide additional information to evaluate our predicted muscle forces. Further characterization of material parameters specific to the different regions of facial skin would improve the model's prediction of tissue strains. We are currently extending the model to include food bolus models for simulations of mastication and swallowing. We are also pursuing simulations to study motor control of speech production as well as the design of maxillofacial reconstructions that predict post-operative orofacial function in addition to post-operative aesthetics.

Acknowledgments We gratefully thank Pierre Badin at Gipsa-Lab Grenoble for providing the CT data used for subject specific morphology. We also thank Poul Nielson and collaborators at the Auckland Bioengineering Institute for their assistance with the subject-specific material properties experiments. We also thank ANSYS for making licenses available. Funding for this work has been provided by the National Science and Engineering Research Council of Canada and the Michael Smith Foundation for Health Research.

References

1. Delp, S. L., Anderson, F. C., Arnold, A. S., Loan, P., Habib, A., John, C. T., et al. (2007). Opensim: Open-source software to create and analyze dynamic simulations of movement. *IEEE Transactions on Biomedical Engineering*, *54*(11), 1940–1950.
2. Blemker, S. S., Asakawa, D. S., Gold, G. E., & Delp, S. L. (2007). Image-based musculoskeletal modeling: Applications, advances, and future opportunities. *Journal of Magnetic Resonance Imaging*, *25*(2), 441–451.
3. Terzopoulos, D., & Waters, K. (1990). Physically-based facial modelling, analysis, and animation. *The Journal of Visualization and Computer Animation*, *1*(2), 73–80.
4. Sifakis, E., Neverov, I., & Fedkiw, R. (2005). Automatic determination of facial muscle activations from sparse motion capture marker data. In *ACM Transactions on Graphics (TOG), ACM* (Vol. 24, pp. 417–425).
5. Hung, A. P. L., Wu, T., Hunter, P., & Mithraratne, K. (2011). Simulating facial expressions using anatomically accurate biomechanical model. In *SIGGRAPH Asia 2011 Posters, ACM*, p. 29.
6. Gerard, J. M., Perrier, P., & Payan, Y. (2006). 3d biomechanical tongue modeling to study speech production. In *Speech production: Models, phonetic processes, and techniques* (pp. 85–102). New York: Psychology Press.
7. Buchaillard, S., Perrier, P., & Payan, Y. (2009). A biomechanical model of cardinal vowel production: Muscle activations and the impact of gravity on tongue positioning. *The Journal of the Acoustical Society of America*, *126*(4), 2033–2051.
8. Stavness, I., Lloyd, J. E., Payan, Y., & Fels, S. (2011). Coupled hard-soft tissue simulation with contact and constraints applied to jaw-tongue-hyoid dynamics. *International Journal for Numerical Methods in Biomedical Engineering*, *27*(3), 367–390.
9. Nazari, M. A., Perrier, P., Chabanas, M., & Payan, Y. (2011). Shaping by stiffening: A modeling study for lips. *Motor Control*, *15*(1), 141–168.
10. Stavness, I., Nazari, M. A., Perrier, P., Demolin, D., & Payan, Y. (2013). A biomechanical modeling study of the effects of the orbicularis oris muscle and jaw posture. *Journal of Speech, Language, and Hearing Research*, *56*, 878–890.
11. Flynn, C., Stavness, I., Lloyd, J. E., & Fels, S. (2013a). A finite element model of the face including an orthotropic skin model under in vivo tension. *Computer Methods in Biomechanics and Biomedical Engineering* (in press).
12. Zhang, Q., Liu, Z., Quo, G., Terzopoulos, D., & Shum, H. Y. (2006). Geometry-driven photorealistic facial expression synthesis. *IEEE Transactions on Visualization and Computer Graphics*, *12*(1), 48–60.
13. Mori, M., MacDorman, K., & Kageki, N. (2012). The uncanny valley (from the field). *IEEE Robotics & Automation Magazine*, *19*(2), 98–100.
14. Beeler, T., Hahn, F., Bradley, D., Bickel, B., Beardsley, P., Gotsman, C., Sumner, R. W., & Gross, M. (2011). High-quality passive facial performance capture using anchor frames. In: *ACM Transactions on Graphics (TOG), ACM* (Vol. 30, p. 75).
15. Hannam, A. (2011). Current computational modelling trends in craniomandibular biomechanics and their clinical implications. *Journal of Oral Rehabilitation*, *38*(3), 217–234.
16. Chabanas, M., Luboz, V., & Payan, Y. (2003). Patient specific finite element model of the face soft tissues for computer-assisted maxillofacial surgery. *Medical Image Analysis*, *7*(2), 131–151.
17. Mollemans, W., Schutyser, F., Nadjmi, N., Maes, F., Suetens, P., et al. (2007). Predicting soft tissue deformations for a maxillofacial surgery planning system: from computational strategies to a complete clinical validation. *Medical Image Analysis*, *11*(3), 282–301.
18. Claes, P., Vandermeulen, D., De Greef, S., Willems, G., Clement, J. G., & Suetens, P. (2010). Computerized craniofacial reconstruction: conceptual framework and review. *Forensic science international*, *201*(1), 138–145.

19. Rohner, D., Guijarro-Martinez, R., Bucher, P., & Hammer, B. (2013). Importance of patient specific intraoperative guides in complex maxillofacial reconstruction. *Journal of Cranio-Maxillofacial Surgery*, *41*(5), 382–390.
20. Nazari, M. A., Perrier, P., Chabanas, M., & Payan, Y. (2010). Simulation of dynamic orofacial movements using a constitutive law varying with muscle activation. *Computer Methods in Biomechanics and Biomedical Engineering*, *13*(4), 469–482.
21. Hannam, A. G., Stavness, I., Lloyd, J. E., & Fels, S. (2008). A dynamic model of jaw and hyoid biomechanics during chewing. *Journal of Biomechanics*, *41*(5), 1069–1076.
22. Peck, C., Langenbach, G., Hannam, A., et al. (2000). Dynamic simulation of muscle and articular properties during human wide jaw opening. *Archives of Oral Biology*, *45*(11), 963–982.
23. Bucki, M., Lobos, C., & Payan, Y. (2010a). A fast and robust patient specific finite element mesh registration technique: Application to 60 clinical cases. *Medical Image Analysis*, *14*(3), 303–317.
24. Bucki, M., Nazari, M. A., & Payan, Y. (2010b). Finite element speaker-specific face model generation for the study of speech production. *Computer Methods in Biomechanics and Biomedical Engineering*, *13*(4), 459–467.
25. Flynn, C., Taberner, A., Nielsen, P., & Fels, S. (2013b). Simulating the three-dimensional deformation of in vivo facial skin. *Journal of the Mechanical Behavior of Biomedical Materials* (in press).
26. Schiavone, P., Promayon, E., & Payan, Y. (2010). Lastic: A light aspiration device for in vivo soft tissue characterization (pp. 1–10). In *Biomedical simulation*. New York: Springer.
27. Blemker, S. S., Pinsky, P. M., & Delp, S. L. (2005). A 3d model of muscle reveals the causes of nonuniform strains in the biceps brachii. *Journal of Biomechanics*, *38*(4), 657–665.
28. Weiss, J. A., Maker, B. N., & Govindjee, S. (1996). Finite element implementation of incompressible, transversely isotropic hyperelasticity. *Computer Methods in Applied Mechanics and Engineering*, *135*(1), 107–128.
29. Gerard, J. M., Ohayon, J., Luboz, V., Perrier, P., & Payan, Y. (2005). Non-linear elastic properties of the lingual and facial tissues assessed by indentation technique: Application to the biomechanics of speech production. *Medical Engineering & Physics*, *27*(10), 884–892.
30. Mooney, M. (1940). A theory of large elastic deformation. *Journal of applied physics*, *11*(9), 582–592.
31. Rivlin R (1948) Large elastic deformations of isotropic materials. iv. Further developments of the general theory. *Philosophical Transactions of the Royal Society of London Series A, Mathematical and Physical Sciences241*(835), 379–397.
32. Fung, Y. C. (1993). *Biomechanics: Mechanical Properties of Living Tissues*. New York: Springer.
33. Borges, A. F. (1984). Relaxed skin tension lines (rstl) versus other skin lines. *Plastic and Reconstructive Surgery*, *73*(1), 144–150.
34. Lloyd, J. E., Stavness, I., Fels, S. (2012). ArtiSynth: A fast interactive biomechanical modeling toolkit combining multibody and finite element simulation. In Y. Payan (Ed.), *Soft tissue biomechanical modeling for computer assisted surgery* (Vol. 11, pp. 355–394). New York: Springer.
35. MacNeilage, P. F., & Davis, B. L. (2000). On the origin of internal structure of word forms. *Science*, *288*(5465), 527–531.
36. Stavness, I., & Kim, S. (2013). Towards a multi-compartment finite-element model of the supraspintus muscle (pp. 115–116). In *Computer Methods in Biomechanics and Biomedical Engineering*.